Localization of plasmon modes in a 2D photonic nanostructure with a controlled disorder

T. Ung, X. Quélin, J. Laverdant, R. Fulcrand, J.-P. Hermier, S. Buil

Research Article | Vol. 29, No. 13 / 21 June 2021 / Optics Express 20776
Optics EXPRESS

Localization of plasmon modes in a 2D photonic nanostructure with a controlled disorder

T. P. L. Ung,[1] X. Quélin,[1] J. Laverdant,[2] R. Fulcrand,[2] J.-P. Hermier,[1] and S. Buil[1,*]

[1] Université Paris-Saclay, UVSQ, CNRS, GEMaC, 78000, Versailles, France
[2] Institut Lumière Matière, Université Claude Bernanrd Lyon I, CNRS,Université de Lyon, F- 69622 Villeurbanne, France
[*] stephanie.buil@uvsq.fr

Abstract: In this paper, we focus on the optical properties of disordered hole arrays etched in a gold thin film. The disorder is induced and controlled using hole displacements following a Gaussian distribution and starting from a periodic array. The nanostructures present a transition from ordered arrays to short-range ordered arrays and random arrays by increasing the disorder amount. The associated optical properties are characterized in far and near fields by complementary approaches (absorption spectroscopy, classical scanning near field optical microscopy (SNOM) and Finite Difference Time Domain (FDTD) simulations). By increasing the disorder, a broadened absorption up to 30% in the far-field is achieved. Experiments in agreement with FDTD simulations point out the energy localization induced by the disorder and the dependence on the amount of disorder and on the excitation wavelength. By using a controlled disorder, we also show that the effect of these two parameters is also closely linked.

1. Introduction

Optical nanostructures raise a great interest in the wide field of nanosciences [1–3]. The design of such devices covers a wide range of applications such as quantum information processing, solar cells for photovoltaic or efficient analytical sensing in chemistry and molecular biology [4,5]. As another example, the enhancement of the coupling between light and matter becomes an essential research domain of nanophotonics. Many applications are based on the localization of the electromagnetic energy in small volumes inside the nanostructure leading to strong electric field enhancements. The control of the electromagnetic environment can be performed through periodic dielectric or metallic devices.

A complementary approach relies on random structures. In his pioneer work, P. W. Anderson observed the unusual transport properties of disordered materials leading to the so-called Anderson localization phenomenon [6]. It results from wave interferences generated by multiple-scattering paths induced by defects in the solid [7–10]. In optics, low-dimensional disordered structures (one-dimension, 1D, or two-dimension, 2D) are investigated by many groups to achieve strong localization of light [11–16]. Two kinds of disorder can be generated, one using completely random patterns [17–19] and a second one starting from a periodic nanostructure [13,20,21]. In this case, the disorder can be controlled by modifying the periodic arrangement with different distribution functions, for example a radial function [22] or a gaussian one [23–28].

In this paper, starting from a periodic arrangement of nanoholes in a thin gold film, we apply the second approach in order to continuously vary the amount of disorder. Nanohole arrays in thin metallic films are very interesting nanostructures as localized surface plasmons (LSPs) and surface propagating plasmons (SPPs) can interact through the metallic layer [29–31]. The disorder can then induce multiple scattering and interferences of SPPs leading to energy localization [32–34]. The effect of disorder (following a gaussian distribution) on the optical properties is investigated through absorption spectroscopy and classical scanning near field optical microscopy

#424970 https://doi.org/10.1364/OE.424970
Journal © 2021 Received 29 Mar 2021; revised 25 May 2021; accepted 25 May 2021; published 17 Jun 2021

Optics EXPRESS

(SNOM) and compared to FDTD simulations. We observe that energy localization appears even for a weak disorder and, more importantly, investigate on how the level of disorder and the excitation wavelength modify in a correlated way the energy confinement. We show that localization effects appear as soon as a slight disorder is introduced but that for a particular wavelength, the localization effects tend to saturate above a particular level of disorder.

2. Fabrication and characterization of the array disorder

To quantify the disorder, we use a periodic array as a reference and move each hole from its initial position by a distance following a Gaussian distribution. The amount of disorder is controlled through the standard deviation of the Gaussian distribution. The disorder level δ is defined as the ratio between the standard deviation σ of the Gaussian distribution of the hole displacement and the periodicity p of the original ordered hole array:

$$\delta = \frac{\sigma}{p} \tag{1}$$

We choose to start from a periodicity p equal to 425 nm and a hole diameter of 150 nm in a thin gold film with a thickness around 40 nm (around the skin depth of gold in the visible range). These parameters have been chosen due to the plasmon resonance appearing around 620 nm that has been used to study the ordered arrays by the coupling with nanoemitters in a previous work [35]. The size of the holes has been fixed due to limitations induced by the near field optics resolution which is around 150 nm. To avoid overlaps between holes, δ ranges from 0 % to 19 %. The fabrication of the 15×15 hole array on a gold film with a thickness of 38 nm is described in [35]. Fig. 1(a) presents how the disorder is generated starting from the ordered structure. The yellow circles represent an example of displacement of the holes from their initial position. The Fig. 1(b) plots the gaussian distributions of this displacement when increasing the standard deviation.

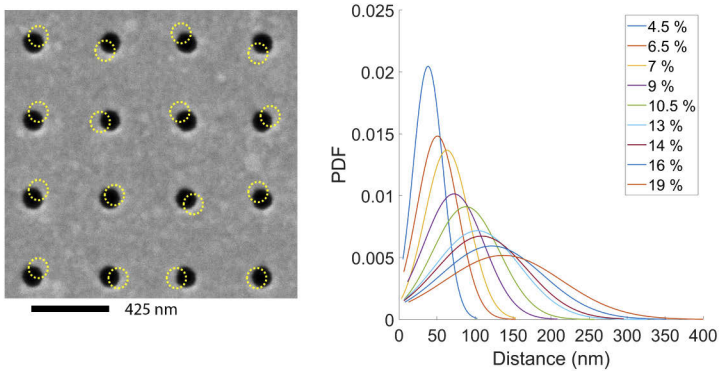

Fig. 1. (a) FIB-SEM topographic image of the 15×15 ordered hole array, periodicity p=425 nm and hole diameter d=150 nm. The yellow circles show an example of displacement for each hole. (b) Gaussian distributions with increasing standard deviation and corresponding degree of disorder δ.

The topographies of 3 typical arrays are displayed on the top of Fig. 2. In order to quantify the evolution of the disorder with the parameter δ, we plotted the 2D autocorrelation function (ACF) $C(\Delta X, \Delta Y)$ of the SEM images intensity $I(x, y)$. It writes:

$$C(\Delta X, \Delta Y) = \langle \delta I_{norm}(x, y) \delta I_{norm}(x + \Delta X, y + \Delta Y) \rangle \tag{2}$$

with $\delta I_{norm}(x, y) = [I(x, y) - \langle I(x, y) \rangle] / \langle I(x, y) \rangle$. For time series, the ACF provides a mathematical image of the level of similarity between a variable value and its future or past value. C is equal to

Optics EXPRESS

1 for a perfect correlation and to 0 in the absence of correlations. The 2D ACF is its counterpart for two dimension spatial structures. In our case, it gives the correlation between the positions of the holes and illustrates how the order decreases when considering holes that are more and more distant from each other. Numerically, the 2D ACF is calculated by using the Wiener–Khintchine theorem and 2D fast Fourier transform and inverse fast Fourier transform functions [36].

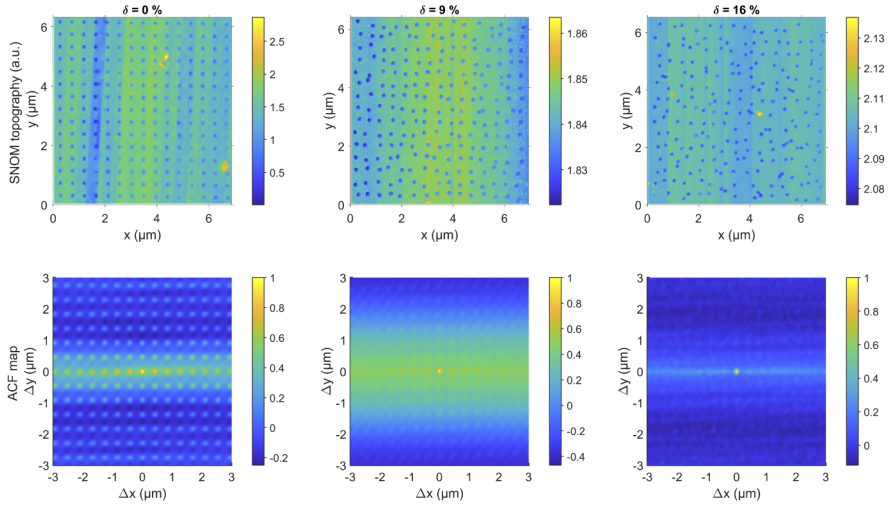

Fig. 2. Top line: topography of three arrays with δ = 0, 9 and 16 % (from left to right). Bottom line: corresponding deviation to 1 of 2D-ACF .

For the periodic structure (δ = 0%), the 2D-ACF exhibits the periodicity of the array. This periodicity vanishes as the disorder increases. For a disorder level of δ = 9%, a short-range order still exists in the structure as the oscillations of the function are weaker but still remain. This order is no more visible when the disorder reaches δ = 16% as the oscillations of the 2D-ACF have disappeared.

3. Evolution of the optical properties with disorder

The absorption of the arrays was measured with a confocal microscope (IX 71, Olympus) illuminated with a white laser (superK EXTREME-White EXW-12) and coupled to a spectrophotometer (Princeton Instruments SP2750). The wavelength of the white laser ranges from 530 nm to 760 nm with a narrow linewidth (FWHM of 1 nm). The absorption is deduced from the reflection and transmission measurements. The absorption of different arrays (δ = 0%, δ = 9%, δ = 13% and δ = 16%) is displayed and compared to the absorption of a flat gold film with the same thickness (Fig. 3(a)). The enhancement of the absorption of the ordered hole array with two absorption peaks reaching 40% has already been observed and originates from the coexistence of Surface Plasmons Polaritons (SPPs) and Localized Surface Plasmons (LSPs) [31]. On this kind of nanostructures, LSPs generated by the holes can couple together through SPPs propagating on the gold film [31,32]. Their optical properties are then very sensitive to the periodicity of the array and it has been shown that the absorption maximum is redshifted when the periodicity is increased. In a previous work [35], we used this property and FDTD simulations to tune the array geometry so the first peak resonance wavelength matches the one of the fluorescence of nanocrystals. This optical sensitivity to interhole separation explains that the absorption peaks decreases when the disorder increases as it is observed on Fig. 3, and as reported for disordered metallic photonic crystal slabs showing, as in our case, an uncorrelated disorder [37]. This behavior can be connected to the order in the array observed on the ACF of the topography. For

Optics EXPRESS

an intermediate disorder, the short-range order is still present as observed on the ACF of the topography whereas it is completely suppressed for the highest disorder (δ = 16%). The first absorption peak centered around 610 nm seems to follow the short range-order. It decreases as the short range order reduces and completely vanishes when the short-range order disappears. It is clearly influenced by the periodicity of the array and can be attributed to diffraction of SPPs by the array. The second peak centered around 740 nm seems more robust to disorder as it is still visible for the maximum disorder where short-range order has completely disappeared and might be attributed to LSPs of the nanoholes. The optical behavior shows that, as the disorder increases, the absorption observed for the ordered array spreads over the entire wavelength range with a mean value around 25%.

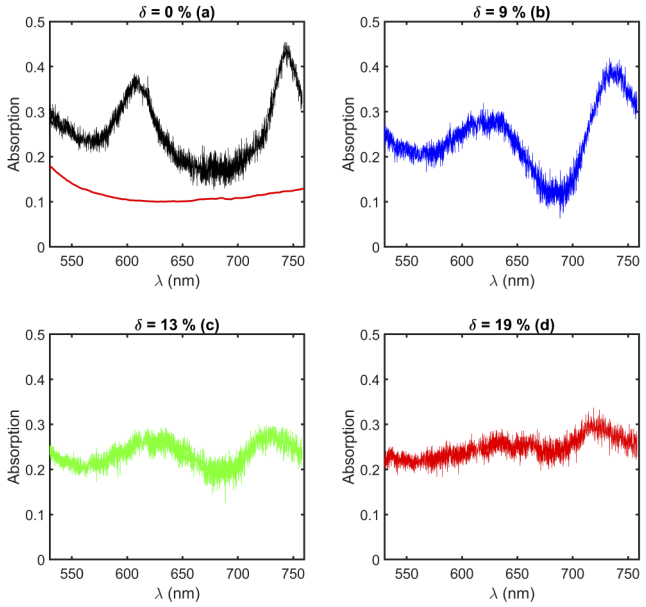

Fig. 3. Absorption spectra between 530 nm and 760 nm of the arrays corresponding to 4 values of δ = 0 % (a), 9 % (b), 13 % (c), and 19 % (d). In (a), the red line shows the absorption spectrum for a flat gold film of the same thickness.

4. Localization of the electromagnetic modes with disorder

To get insight into the mechanisms of the absorption modification in the disordered arrays, it is crucial to determine how the electromagnetic energy is distributed in the nanostructure. For this purpose, optical near field experiments have been carried out and compared to numerical simulations. A classical aperture scanning near field optical microscope (SNOM) was used to map the near electric field of these plasmonic nanostructures (see Fig. 4). The classical SNOM is based on an inverted microscope (IX 71, Olympus) and adapted to a commercial SNOM head (NTMDT). A tuning fork supporting a metal-coated dielectric tip having an aperture diameter of 100 nm is attached to a piezoelectric scanner in order to perform nanometric displacements in the three space directions (x, y, z). In addition, the sample holder is connected to a second piezoelectric scanner with two translation axes (x, y) in order to displace the sample in the horizontal plane. The excitation which comes from the super-continuum laser is focused on the sample by an air objective (Olympus-LMPLFLM 50x) with a numerical aperture = 0.5. The near field transmission signal of the plasmonic nano-structures is collected through the SNOM fiber and detected by an TTi QL355 avalanche photodiode. The near field distribution has been

Optics EXPRESS

studied for arrays with disorder δ ranging from 0 % to 16 % and by varying the wavelength from 590 nm to 730 nm.

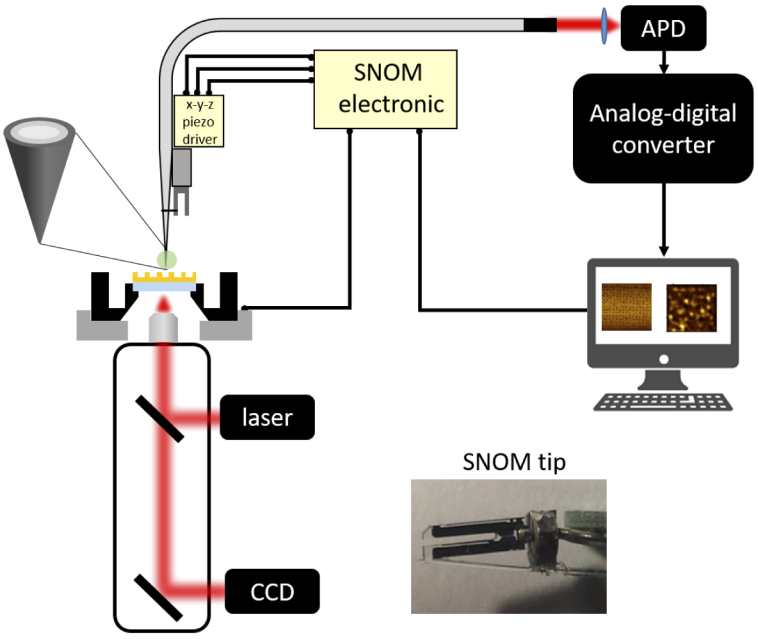

Fig. 4. Schematic representation of the SNOM experimental setup.

4.1. *Influence of the disorder level*

The effect of disorder is first presented on Fig. 5. It shows the evolution of the near field distribution for a wavelength excitation of 660 nm and for 4 levels of disorder. When there is no disorder (δ = 0 %), the near field distribution looks like the topography and the array can be retrieved on the optical near field image. When disorder increases, some areas with a higher intensity randomly appear and dominate the near field distribution for δ=16 %. The array is no more visible on the optical image which is more and more dominated by the localization of the electromagnetic field in small areas. To characterize this evolution, the probability distribution function (PDF) of the intensity is plotted on Fig. 6 (top left), where the experimental SNOM images have been normalized in order to get a minimum value of 1 for the intensity (we checked that the minimum intensity detected is far from the null signal in order to avoid any unphysical result). As the disorder increases, the distribution becomes more and more asymmetrical and a large tail on the side of the highest intensities appears. The peak of the distribution is also slightly shifted to higher values of the intensities. The tail of the distribution corresponds to the electromagnetic energy localization induced by disorder. This energy localization appears as soon as a slight disorder is introduced in the array. As the disorder grows the near-field localization becomes stronger. The evolution of the tail of the distribution reflects that few areas with higher intensities show up. Nevertheless, the energy localization rise seems to slow down when the disorder increases. This localization comes from the interferences of the SPPs scattered by nanoholes. The randomness gives rise to complex scattering leading to plasmon localization.

For comparison, we did the same analysis for a wavelength of 730 nm (for the two wavelengths, 660 nm and 730 nm, the localization effects are typical but different enough to show the wavelength-dependent behavior of the localization). The PDF deduced from optical near field images after normalization are presented on Fig. 6 (top right). The same behavior as for 660

Optics EXPRESS

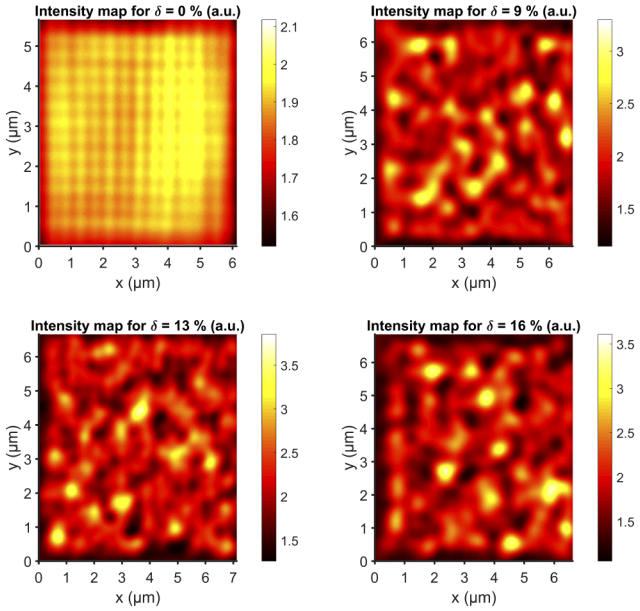

Fig. 5. SNOM images for 4 amounts of disorder δ (0 %, 9 %, 13 %, and 16 %). For δ = 0%, the image shows the part where the holes were the best visible.

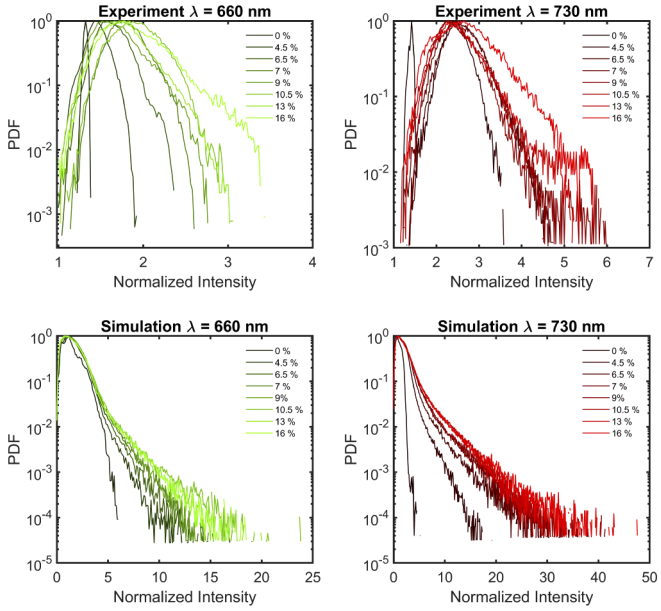

Fig. 6. Experimental PDF of the intensity for λ=660 nm (top left) and 730 nm (top right) and δ increasing from δ = 4.5%, δ = 6.5%, δ = 7%, δ = 9%, δ = 10.5%, δ = 13%, and δ = 16%. For δ = 4.5% for λ=730 nm, the image shows the part where the holes were the best visible. Simulated PDF (bottom) of the intensity for the same parameters. For each plot, the color of the curves is lighter the larger δ.

Optics EXPRESS

nm is observed but the energy localization reaches higher values than for 660 nm since higher normalized intensities appear in the PDF.

These experimental results have been compared to FDTD simulations performed with the Lumerical software (for details on these numerical simulations see Ref. [38]). The incident plane wave and the intensity distributions have been deduced from the near field distributions calculated 30 nm above the surface. The results obtained for λ = 660 nm and 730 nm are presented on Fig. 6 (bottom left) and Fig. 6 (bottom right). The simulation predictions first show the same tendencies as the experimental results. The appearance and the increase of a tail toward higher values of the intensities when disorder increases is evidenced. It is however more pronounced than experimentally. Moreover, the peak also remains at the same position and does not shift as experimentally. This discrepancy between experiments and simulations is explained by the limit of the SNOM resolution that is not better than 100 nm due to the size of the tip (the meshing parameter of FDTD maps is 10 nm). Experimentally, the intensity is averaged over areas far larger than the localization observed numerically. Interestingly, in the simulations, we also observe that the effect of disorder is stronger for a higher wavelength. High values of the intensity corresponding to energy localization appear when disorder increases but are more pronounced for the highest wavelengths. In both cases, the localization tends to saturate and increasing the disorder no more boosts the localization. The localization coming from the propagation of SPPs, interferences are stronger when the disorder increases but they are limited by the decay length of SPPs at long distances. For a fixed wavelength there is a maximum level of disorder beyond which the localization no longer increases.

4.2. Influence of the excitation wavelength

To get more insights into the interconnection between the disorder level and the excitation wavelength, the near field distribution has also been studied for a fixed disorder at different wavelengths. In Fig. 7 (left), we present the PDF for a disorder level δ = d16% with wavelengths ranging from 590 nm to 730 nm. For comparison, the PDF obtained by FDTD are presented on Fig. 7 (right). For this disorder, the tail corresponding to energy localization is present in the distribution for all wavelengths. It reaches higher values for longer wavelengths and tends to saturate. We observe that, for a given disorder level, the energy localization increases with the wavelength but more and more slowly. Simultaneously, the spatial hot spot structure may vary with the wavelength. Larger localization lengths could be observed as large wavelength excitations are used, leading to hot spots with a larger size. It could be interesting to study the spatial structure of the hot spots (using for example the 2D ACF of the intensity). However, the spatial resolution of our SNOM setup ($\sim$ 150 nm) is too low to allow us to investigate these modifications. This behavior has recently been observed in short-range order nanoholes arrays [33] by cathodoluminescence experiments. Stronger field enhancements have been attributed to higher wavelengths generated by longer hole-to-hole distances. As the wavelength increases, longer distances can be probed due to the increase of the SPP decay length. These experiments where the level of disorder is increased for a fixed wavelength or where the wavelength is increased for a fixed disorder, confirm that the energy localization that is induced by interfering SPPs waves strongly depends on both parameters and show the limitations for both of them. It shows that the disorder induces plasmon localization that increases with the level of disorder and the wavelength but is limited by the decay length of SPPs.

4.3. Statistical analysis using the 2D autocorrelation function of the near field intensity

Previous papers have shown that calculating the 2D-ACF of the intensity is a very efficient approach to analyze the coupling between light and a structured metallic surface and especially the degree of plasmon localization [20,39]. In Fig. 8 (top line), we plotted the maps we obtained at a wavelength of 660 nm for 4 disorder levels. A section line corresponding to $\Delta Y = 0$ is

Optics EXPRESS

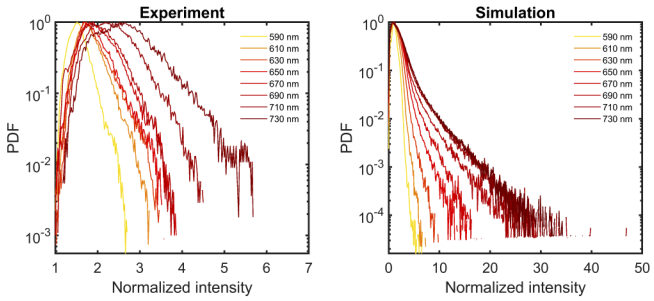

Fig. 7. Experimental PDF of the intensity for δ=16% and λ ranging between 590 nm and 730 nm (left). Simulated PDF of the intensity for the same values (right). For each subfigure, the color of the curves is more dark red as the wavelength is large.

also shown (bottom line). For δ = 0%, the 2D-ACF shows a periodic order with a periodicity corresponding to the array period (the 2D-ACF was performed on a croped image of 5 × 5 μm of the array where the holes were best visible on the optical image). As for the topography, when δ increases, the pattern as well as the symmetry along the x and y axis gradually disappear. The ACF is normalized by the variance σ^2 of the intensity which is given inside each bottom subfigure. We then observe that the variance of the intensity distribution grows with disorder. This dependency shows the transition from short-range order to random array dominated by localization and reflects the influence of the high field intensities induced by plasmon localization.

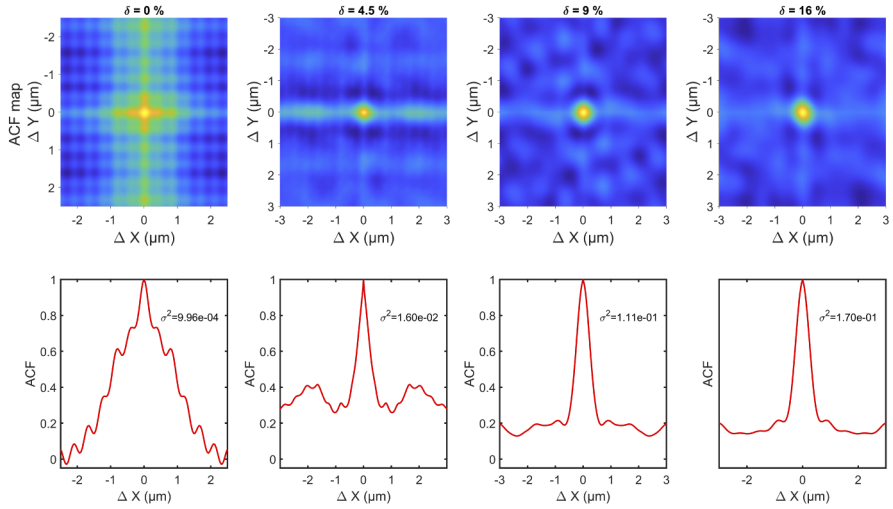

Fig. 8. Experimental deviation to 1 of the 2D-ACF of the intensity for δ = 0 %, 4.5 %, 9 %, and 16 %.

5. Conclusion

In conclusion, our results based on complementary experimental and numerical approaches detail the impact of a controlled disorder generated from an ordered array. The disorder creates a large broadening of the absorption and localization of the electromagnetic field on the surface due to multiple scattering and interferences of SPPs. This localization effect appears as soon as slight disorder is introduced and increases with the disorder level and with the wavelength. For longer wavelengths, plasmons can propagate over larger distances and generate stronger localization

Optics EXPRESS

effects. Interestingly, the approach based on an adjusted disorder at last enables to demonstrate that there is a close interconnection between the wavelength and the amount of disorder on the localization properties. This study shows that for a particular wavelength, increasing the disorder does not increase the localization of the electromagnetic field.

Disclosures. The authors declare that there are no conflicts of interest related to this article.

Data availability. Data underlying the results presented in this paper are not publicly available at this time but may be obtained from the authors upon reasonable request.

References

1. K. Uwe and M. Vollmer, *Optical Properties of Metal Clusters*, vol. 25 (Springer-Verlag Berlin Heidelberg, 1995).
2. B. Lamprecht, G. Schider, R. T. Lechner, H. Ditlbacher, J. R. Krenn, A. Leitner, and F. R. Aussenegg, "Metal Nanoparticle Gratings: Influence of Dipolar Particle Interaction on the Plasmon Resonance," Phys. Rev. Lett. **84**(20), 4721–4724 (2000).
3. T. Klar, M. Perner, S. Grosse, G. von Plessen, W. Spirkl, and J. Feldmann, "Surface-Plasmon Resonances in Single Metallic Nanoparticles," Phys. Rev. Lett. **80**(19), 4249–4252 (1998).
4. P. Lodahl, S. Mahmoodian, and S. Stobbe, "Interfacing single photons and single quantum dots with photonic nanostructures," Rev. Mod. Phys. **87**(2), 347–400 (2015).
5. J.-H. Yun, E. Lee, H.-H. Park, D.-W. Kim, W. A. Anderson, J. Kim, N. M. Litchinitser, J. Zeng, J. Yi, M. M. D. Kumar, and J. Sun, "Incident light adjustable solar cell by periodic nanolens architecture," Sci. Rep. **4**(1), 6879 (2015).
6. P. W. Anderson, "Absence of Diffusion in Certain Random Lattices," Phys. Rev. **109**(5), 1492–1505 (1958).
7. G. Bergmann, "Quantitative analysis of weak localization in thin Mg films by magnetoresistance measurements," Phys. Rev. B **25**(4), 2937–2939 (1982).
8. I. M. Lifshits, *Quantum Theory of Solids* (Mir Publishers, Moscow, 1983).
9. P. A. Lee and T. V. Ramakrishnan, "Disordered electronic systems," Rev. Mod. Phys. **57**(2), 287–337 (1985).
10. C. A. Condat, T. R. Kirkpatrick, and S. M. Cohen, "Acoustic localization in one dimension in the presence of a flow field," Phys. Rev. B **35**(10), 4653–4661 (1987).
11. P. Sebbah, D. Sornette, and C. Vanneste, "Anomalous diffusion in two-dimensional Anderson-localization dynamics," Phys. Rev. B **48**(17), 12506–12510 (1993).
12. M. M. Sigalas, C. M. Soukoulis, C.-T. Chan, and D. Turner, "Localization of electromagnetic waves in two-dimensional disordered systems," Phys. Rev. B **53**(13), 8340–8348 (1996).
13. T. Schwartz, G. Bartal, S. Fishman, and M. Segev, "Transport and Anderson localization in disordered two-dimensional photonic lattices," Nature **446**(7131), 52–55 (2007).
14. F. Riboli, P. Barthelemy, S. Vignolini, F. Intonti, A. D. Rossi, S. Combrie, and D. S. Wiersma, "Anderson localization of near-visible light in two dimensions," Opt. Lett. **36**(2), 127–129 (2011).
15. L. Martin, G. Di Giuseppe, A. Perez-Leija, R. Keil, F. Dreisow, M. Heinrich, S. Nolte, A. Szameit, A. F. Abouraddy, D. N. Christodoulides, and B. E. A. Saleh, "Anderson localization in optical waveguide arrays with off-diagonalcoupling disorder," Opt. Express **19**(14), 13636–13646 (2011).
16. D. M. Jovi, Y. S. Kivshar, C. Denz, and M. R. Belic, "Anderson localization of light near boundaries of disordered photonic lattices," Phys. Rev. A **83**(3), 033813 (2011).
17. S. Buil, J. Aubineau, J. Laverdant, and X. Quélin, "Local field intensity enhancements on gold semicontinuous films investigated with an aperture nearfield optical microscope in collection mode," J. Appl. Phys. **100**(6), 063530 (2006).
18. K. Vynck, M. Burresi, F. Riboli, and D. S. Wiersma, "Photon management in two-dimensional disordered media," Nat. Mater. **11**(12), 1017–1022 (2012).
19. V. E. Bochenkov, M. Frederiksen, and D. S. Sutherland, "Enhanced refractive index sensitivity of elevated short-range ordered nanohole arrays in optically thin plasmonic au films," Opt. Express **21**(12), 14763–14770 (2013).
20. W.-B. Shi, L.-Z. Liu, R. Peng, D.-H. Xu, K. Zhang, H. Jing, X.-R. Fan, R.-H. Huang, Q.-J. Wang, and M. Wang, "Strong localization of surface plasmon polaritons with engineered disorder," Nano Lett. **18**(3), 1896–1902 (2018).
21. Y. Nishijima, L. Rosa, and S. Juodkazis, "Surface plasmon resonances in periodic and random patterns of gold nano-disksfor broadband light harvesting," Opt. Express **20**(10), 11466–11477 (2012).
22. T. M. Schmidt, "Engineering of gold and aluminum plasmonic structures: Fabrication and fluorescence enhancement," Phd thesis, Interdisciplinary Nanoscience Center (iNANO), Science and Technology Aarhus University, Denmark (2013).
23. P. D. García, G. Kiršanskė, A. Javadi, S. Stobbe, and P. Lodahl, "Two mechanisms of disorder-induced localization in photonic-crystal waveguides," Phys. Rev. B **96**(14), 144201 (2017).
24. S. Smolka, H. Thyrrestrup, L. Sapienza, T. B. Lehmann, K. R. Rix, L. S. Froufe-Pérez, P. D. García, and P. Lodahl, "Probing the statistical properties of Anderson localization with quantum emitters," New J. Phys. **13**(6), 063044 (2011).
25. A. Javadi, S. Maibom, L. Sapienza, H. Thyrrestrup, P. D. García, and P. Lodahl, "Statistical measurements of quantum emitters coupled to Anderson-localized modes in disordered photonic-crystal waveguides," Opt. Express **22**(25), 30992–31001 (2014).

Optics EXPRESS

26. P. D. García and P. Lodahl, "Physics of Quantum Light Emitters in Disordered Photonic Nanostructures," Ann. Phys. **529**(8), 1600351 (2017).
27. N. Mann, A. Javadi, P. D. García, P. Lodahl, and S. Hughes, "Theory and experiments of disorder-induced resonance shifts and mode edge broadening in deliberately disordered photonic crystal waveguides," Phys. Rev. A **92**(2), 023849 (2015).
28. R. Kumar and S. Mujumdar, "Intensity correlations in metal films with periodic-on-average random nanohole arrays," Opt. Commun. **380**, 174–178 (2016).
29. T. Sannomiya, O. Scholder, K. Jefimovs, C. Hafner, and A. B. Dahlin, "Investigation of plasmon resonances in metal films with nanohole arrays for biosensing applications," Small **7**(12), 1653–1663 (2011).
30. S.-H. Chang, S. K. Gray, and G. C. Schatz, "Surface plasmon generation and light transmission by isolated nanoholes and arrays of nanoholes in thin metal films," Opt. Express **13**(8), 3150–3165 (2005).
31. J. Parsons, E. Hendry, C. P. Burrows, B. Auguié, J. R. Sambles, and W. L. Barnes, "Localized surface-plasmon resonances in periodic nondiffracting metallic nanoparticle and nanohole arrays," Phys. Rev. B **79**(7), 073412 (2009).
32. J. Prikulis, P. Hanarp, L. Olofsson, D. Sutherland, and M. Käll, "Optical spectroscopy of nanometric holes in thin gold films," Nano Lett. **4**(6), 1003–1007 (2004).
33. D. V. Thi, T. Ohno, N. Yamamoto, and T. Sannomiya, "Field localization of hexagonal and short-range ordered plasmonic nanoholes investigated by cathodoluminescence," J. Chem. Phys. **152**(7), 074707 (2020).
34. Y. Zhu, H. Jing, R.-W. Peng, C.-Y. Li, J. He, B. Xiong, and M. Wang, "Realizing Anderson localization of surface plasmon polaritons and enhancing their interactions with excitons in 2d disordered nanostructures," Appl. Phys. Lett. **116**(20), 201106 (2020).
35. T. P. L. Ung, R. Jazi, J. Laverdant, R. Fulcrand, G. Colas des Francs, J.-P. Hermier, X. Quélin, and S. Buil, "Scanning the plasmonic properties of a nanohole array with a single nanocrystal near-field probe," Nanophotonics **9**(4), 793–801 (2020).
36. M. Cesaria, A. Taurino, M. Grazia Manera, and R. Rella, "Short-range ordered 2d nanoholes: lattice-model and novel insight into the impact of coordination geometry and packing on their propagating-mode transmittance features," Nanoscale Adv. **2**(9), 4133–4146 (2020).
37. D. Nau, A. Schönhardt, C. Bauer, A. Christ, T. Zentgraf, J. Kuhl, M. W. Klein, and H. Giessen, "Correlation Effects in Disordered Metallic Photonic Crystal Slabs," Phys. Rev. Lett. **98**(13), 133902 (2007).
38. S. Buil, J. Laverdant, B. Berini, P. Maso, J.-P. Hermier, and X. Quélin, "Fdtd simulations of localization and enhancements on fractal plasmonics nanostructures," Opt. Express **20**(11), 11968–11975 (2012).
39. J. Laverdant, J.-P. Hermier, X. Quelin, and S. Buil, "From scattering regime to strong localization: a statistical analysis of the near-field intensity on random gold films," J. Nanophotonics **7**(1), 073589 (2013).